13.6　　Turbulence in a model tropopause jet: High resolution 3D direct numerical simulations and parameterization

BINSON JOSEPH,[*]
ALEX MAHALOV, BASIL NICOLAENKO, AND KWAN LEUNG TSE
Program in Environmental Fluid Dynamics, Arizona State Univ., Tempe, Arizona

1.　Introduction

Wind shear associated with the midlatitude jet stream acts as a major source of turbulence near the tropopause. Reed (1969) hypothesized that at least a part of the mesoscale struture may be due to such turbulent exchanges. Mesoscale models (such as MM5) do not include a satisfactory parameterization of this tropopausal turbulence (TT). Energetic eddies of vertical scales O(10 m - 100 m) abound in the atmosphere, and they cannot be underestimated as noisy subgrid-scale motions. Reliable simulation of several processes such as clear air turbulence (CAT), electromagnetic wave propagation, stratosphere-troposphere exchange etc. crucially depends on the accuracy of turbulence parameterization on these energetic scales, which lie between the mesoscales and the smaller-scale inertial-range eddies. The use of direct numerical simulations (DNS) and large-eddy simulation (LES) data for validating subgrid parameterization schemes is well-recognized. One important aspect of TT, which has not received attention of DNS/LES community studying shear-stratified turbulence, is the effect of inhomogeneous stratification (doubling of Brunt-Väisälä frequency) across the tropopause.

The first goal of this study is to highlight some results from high-resolution (512 or 1024 vertical levels),

Corresponding author address: Binson Joseph, Dept. of Mathematics, Arizona State University, Tempe, AZ 85287-1804; e-mail: Binson.Joseph@asu.edu

forced numerical simulations of turbulence in a model tropopause jet. A second DNS with a larger value of viscosity has been conducted to obtain nearly balanced budgets (i.e. with negligible residual) for variances and fluxes, for the purpose of evaluating the performance of a simple second-order closure model.

2.　Simulation Methodology

A Boussinesq formulation of the governing equations for the total velocity $\mathbf{U} = (U, V, W)$ and (potential) temperature Θ is used. This system is supplemented with horizontally homogeneous forcing terms Π_U and Π_Θ, which maintain a sustained synoptic-scale jet stream and the doubling of the buoyancy frequency across the tropopause. We are resolving a microscale box centered on a jet stream at the tropopause, for times much shorter than time scales of the synoptic jet dynamics. Π_U is assigned to have a Gaussian form:

$$\Pi_U = \Pi_0 e^{(-(\alpha_1 z)^2)} e^{(-(d/(d-z))^2)} e^{(-(d/(d+z))^2)} e^2 \ ,$$

(where Π_0 is a contant and d is the half-depth of the vertical domain and α_1 a stiffness parameter), with maximum centered at $z = 0$. The source Π_Θ enters through the basic state N profile, which is specified as: $N_b^2(z) = N_o(\partial \Theta_o/\partial z) = N_o^2 K^2(z)$, where N_o is a constant, $\Theta_o = g\beta\Theta_b/N_o$ (where subscript b stands for a basic state variable, g is gravitational acceleration, $\beta = 1/\Theta_R$, and Θ_R is a constant reference temperature) and the nondimensional $K(z)$ profile, which models the doubling of N at the tropopause, has the form:

$K(z) = 1 + [1/(exp(-\alpha_2(z - \delta)) + 1)]$ (where δ can be used to displace N_b-transition layer from the center of the jet ($z = 0$) and α_2 another stiffness parameter). Unless otherwise stated, we set $\alpha_1 = \alpha_2 = \alpha$. As per our convention, N of the time-varying mean state in the simulation is given by $N^2 = N_o(d\langle\theta\rangle/dz) + N_o^2 K^2(z)$. In this paper, $\langle\cdot\rangle$ will always denote a horizontal average. Here, the variable θ, which is the one also used in the numerical code, is defined as $\theta = g\beta\vartheta/N_o$, where ϑ is the time-evolving part of the total potential temperature. Note that θ has unit: length/time.

Simulations, unless otherwise stated, have a resolution $128 \times 128 \times 512$, in a computational domain centered on a jet stream: $x[0, \pi/2]$, $y[0, \pi/2]$, and $z[-5.5, 5.5]$. Periodic boundary conditions are assumed, for all variables, in x and y directions, which enables the use of a standard pseudo-spectral (Fourier) method in the horizontal. Absorbing boundary condition, in the vertical, is implemented as a sponge layer starting at $z = \pm2.75$. In the vertical direction, a domain decomposition method, choosing fourth order Lagrange polynomials at Gauss-Lobatto-Legendre points in subdomains, is used (cf. Tse et al. 2001, hereafter TMNF). The spacing of subdomains is nonuniform so that a high resolution is maintained towards the center of the jet. The width of the subdomains, for $-1/\alpha < z < 1/\alpha$, is 0.004 (thus average vertical grid spacing, in this region, is about 0.001, which at real tropopause region corresponds to O(10 m)) and then gradually increases towards the edges of the domain. The time discretization follows the usual splitting procedure. The simulation is initiated from infinitesimal values. Parameters used in the present DNS are: kinematic viscosity $\nu = 10^{-4}$, thermal diffusivity $\kappa = 1.41 \times 10^{-4}$, $\Pi_0 = 0.2$, $\alpha = 16$, $N_o = 0.2$, and $\delta = 0$.

3. DNS Results

Results are reported, after long-time integration, when the statistics and budgets do not change appreciably in time (i.e. quasi-equilibrium). In all figures to follow, a rescaled vertical coordinate $Z = z\alpha$ is used. The turbulent mean profiles at quasi-equilibrium, shown in Fig. 1a-b, have large-scale features resembling those of a synoptic-scale tropopause jet and doubling of buoy-
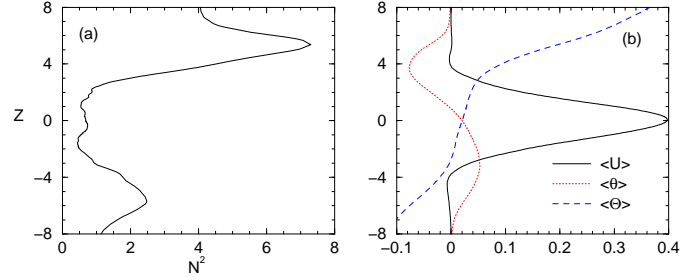

Figure 1: Vertical profiles from DNS: (a) squared Brunt-Väisälä frequency (N^2; normalized by N_o^2) (b) mean streamwise velocity ($\langle U\rangle$), mean perturbation temperature $\langle\theta\rangle$, and mean total temperature $\langle\Theta\rangle$.
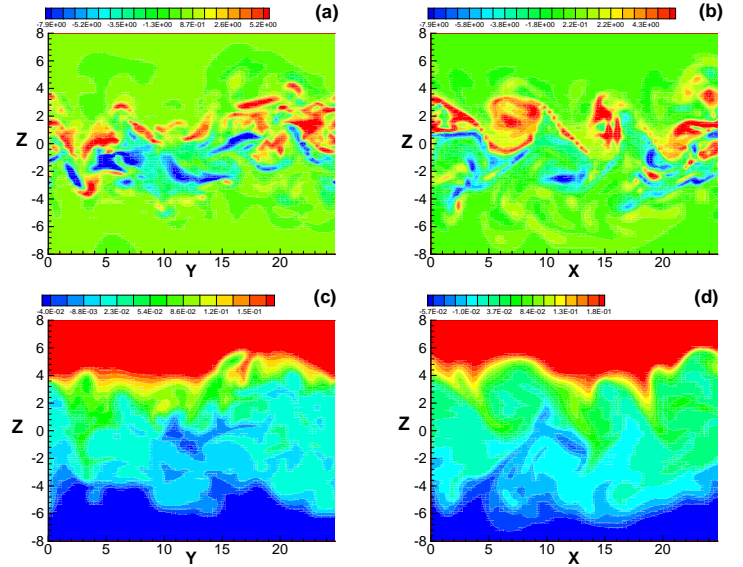

Figure 2: Vertical cross-sections of instantaneous fields: (a) spanwise vorticity on central $Y - Z$ plane ($x = \pi/4$) (b) spanwise vorticity on central $X - Z$ plane ($y = \pi/4$) (c) total temperature in the central $Y - Z$ plane ($x = \pi/4$) (d) total temperature in the central $X - Z$ plane ($y = \pi/4$).

ancy frequency across the tropopause. The formation of an N^2-notch is a noteworthy feature because of its significance in wave emission process (cf. Sutherland and Peltier 1995; Lott and Teitelbaum 1992). The developed nature of three-dimensional (3D) turbulence, and associated mixing is evident from Fig. 2, which shows cross-sections of spanwise vorticity and total temperature. Remnants of Kelvin-Helmholtz (KH) billow structures are discernible in Fig. 2b. Comparable magnitudes of variances, $\langle u'^2 \rangle$, $\langle v'^2 \rangle$, and $\langle w'^2 \rangle$ (primes denoting deviations from the mean $\langle \cdot \rangle$), also exemplify developed 3D turbulence (Fig. 3a). While $\langle u'^2 \rangle$ and $\langle v'^2 \rangle$) peaks on either side of the jet, $\langle w'^2 \rangle$ peaks near the center of the jet. The peaks of temperature variance, $\langle \theta'^2 \rangle$, are located further away from the jet in the vicinity of N^2-bulges (cf. Fig. 1a and Fig. 3a). Vertical momentum flux $\langle u'w' \rangle$ is everywhere downgradient (Fig. 3b). Vertical heat flux $\langle \theta'w' \rangle$ is also mostly downgradient.

The vertical profiles of Richardson number (defined as $Ri_g = N^2/S^2$, where $S^2 = (\partial \langle U \rangle / \partial z)^2 + (\partial \langle V \rangle / \partial z)^2$) and buoyancy-modified Reynolds number (defined as $Re_b = \epsilon/(\nu N^2) = (L_o/L_k)^{4/3}$, where $\epsilon = \nu \langle |\nabla u'|^2 + |\nabla v'|^2 + |\nabla w'|^2 \rangle$, the Ozmidov scale ($L_o$) is given by $L_o^2 = \epsilon/N^3$, and the Kolmogorov microscale is $L_k = (\nu^3/\epsilon)^{1/4}$) are shown in Fig. 4a. The double minima of Ri_g on either side of the jet is in agreement with observations by Bedard et al. (1986) during a CAT event. Both Ri_g and Re_b profiles show that jet core regions are strongly turbulent. The value of Re_b in the turbulent core is O(1000). The point where Re_b becomes O(1) marks the collapse of turbulence by stable stratification (Phillips 1991). Wave dynamics is expected to be dominant in this region. The profiles of L_o, L_k, the dissipation scale (defined as $L_d = q^3/\epsilon$, where $q^2 = \langle u'^2 + v'^2 + w'^2 \rangle$), and the Corrsin-Tatarski scale (defined as $L_t = \epsilon/S^3$) are presented in Fig. 4b. While L_t shows minima in the jet core shear zones (as Ri_g), L_o exhibits peaks in these zones (similar to Re_b). The former behavior is consistent with L_t estimated by Eaton and Nastrom (1998), from radar measurements, who also noted that L_t increases away from the tropopause (cf. their Figure 4). The behavior of L_o in our DNS is in qualitative agreement with the behavior of L_{out} (outer scale of turbulence) estimated by Muschinski (1997) (see his Figure 15), from radar and
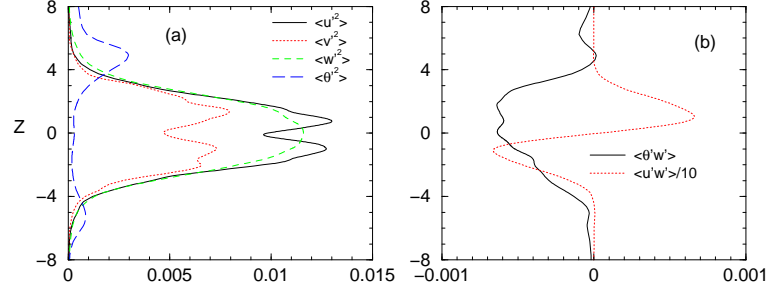

Figure 3: DNS profiles: (a) streamwise velocity variance $\langle u'^2 \rangle$ (solid), spanwise velocity variance $\langle v'^2 \rangle$ (dotted), vertical velocity variance $\langle w'^2 \rangle$ (dashed), temperature variance $\langle \theta'^2 \rangle$ (long-dotted) (b) heat flux $\langle \theta'w' \rangle$ (solid), momentum flux, $\langle u'w' \rangle$ (dotted).
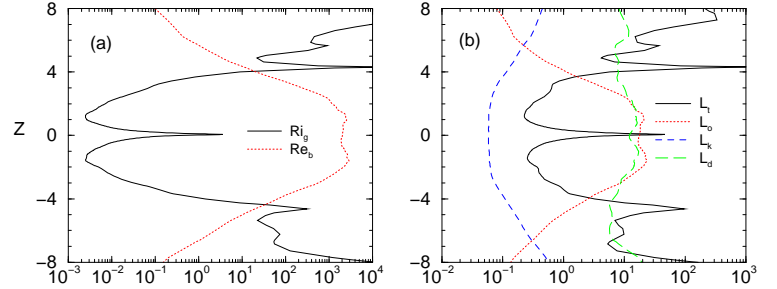

Figure 4: Mean DNS profiles: (a) gradient Richardson number, Ri_g (solid), buoyancy Reynolds number, Re_b (dotted) (b) length scales L_t (solid), L_o (dotted), L_k (dashed), L_d (long-dashed).

radiosonde measurements, who also noted that his L_{out} was not found to correlate well with Ri_g.

Figure 5 shows the scaling, with respect to Ri_g, of flux Richardson number (Ri_f), defined as
$Ri_f = [-N_o \langle w'\theta' \rangle]/[\langle u'w' \rangle (d\langle U \rangle/dz) + \langle v'w' \rangle (d\langle V \rangle/dz)]$,
a key parameter in turbulence modeling, for the standard DNS and for the DNS conducted at doubled resolution ($256 \times 256 \times 1024$). The data for $Z > 0$ and $Z < 0$ are distinguished using circle and triangle symbols, respectively. For each symbol, a different color is used to identify data points for which $N^2 > 0.75$ (black or green) and those with $N^2 < 0.75$ (red or blue). We
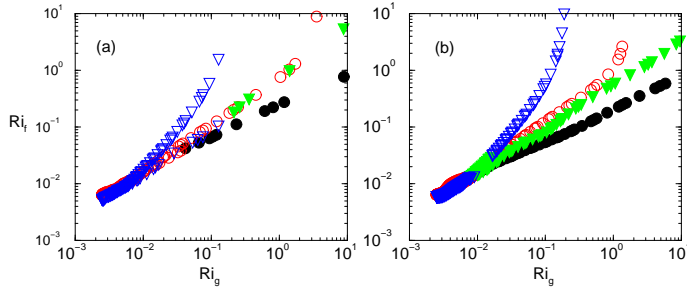
3

Figure 5: Scaling of flux Richardson number (Ri_f) with gradient Richardson number (Ri_g) in DNS with vertical levels: (a) 512 (b) 1024. Data points with $Z > 0$ are circles, and those with $Z < 0$ are triangles. Filled symbols (black or green) denote data points for which $N^2 > 0.75$ and unfilled symbols (red or blue) for those with $N^2 < 0.75$.

note that multiple branches (3 or 4) in the scaling of Ri_f versus Ri_g is a resolution independent feature in our results, which calls for some degree of caution from the part of experimenters. Since some of the branches can be delineated, with respect to an asymmetry in stratification about $Z = 0$, it follows that an improvement in Ri_g-based mixing parameterization might result if the $Ri_f - Ri_g$ formulae are fitted, separately, from field data above and below the tropopause. Note that, in Fig. 5b, different branches are further delineated with respect to the strength of stratification (here choosing a critical value of $N^2 = 0.75$).

Another DNS, with $\nu = 10^{-3}$, has been conducted to arrive at a quasi-equilibrium dataset, with very nearly balanced budgets. The turbulent buoyancy Reynolds number is O(100) for this simulation (not shown). Profiles of variances and fluxes, from this DNS, are shown in Fig. 6. Note that the double peaks in the streamwise velocity variance is not a well-developed feature at this lower value of Reynolds number, in contrast to the DNS at a higher Re_b (cf. Fig. 3a). The budgets of variances and fluxes, shown in Fig. 7, do not have significant residuals. It may be noted that transport term (TR), in this nearly balanced DNS dataset, is a significantly large term even in the TKE budget (not shown). It acts to transfer TKE from shear production zones, on either side of the jet, to the innermost core of the jet, and also to the outer edges of the mixing layer.

4. Second-order closure: preliminary results

As a first step, it is useful to evaluate the performance of a Mellor-Yamada type second-order closure model (Chasnov and Tse 2001; Mellor and Yamada 1982), in order to identify those terms which would require more careful modeling strategies. In the present model, pressure-strain (redistribution) terms are modeled using return-to-isotropy assumption and another term involving mean shear contribution, dissipation terms (only for variances) using Kolmogorov's hypothesis of local, small-scale isotropy, and the transport terms, collectively, using an isotropic, gradient-transfer hypothesis. There are several length scales appearing in the model, which are all assumed to be proportional to a master length scale. The proportionality constants is determined so as to obtain best agreement between modeled and DNS terms. Our choice of the master length scale is to use the vertical profile of horizontally averaged dissipation scale, L_d, computed from the DNS dataset (cf. Fig. 4b). In practical mesoscale modeling applications, this choice may be a concern. One plausible suggestion will be to consider a dissipation scale computed from the small scales of the resolved motions in the mesoscale model. Because of horizontal homogeneity, the model has variability only in the vertical direction. Since a term involving $\langle u'\theta' \rangle$ (BP in Fig. 7e), and dissipation terms in budgets of $\langle u'w' \rangle$ and $\langle \theta'w' \rangle$ are found to be very small in the DNS dataset, they are ignored in the present closure modeling. Thus, a system of 8 equations (4 for variances, 2 for vertical fluxes, and 2 for mean quantities) has to be solved, with suitably tuned constants, until a quasi-equilibrium state is reached. These equations were integrated using a second-order Runge-Kutta scheme.

Profiles of means, variances, and fluxes from the closure model are shown in Fig. 8. Most qualitative features, except the peaks of $\langle u'^2 \rangle$ at either sides of the jet, is comparable to the DNS results (cf. Fig. 6). Al-
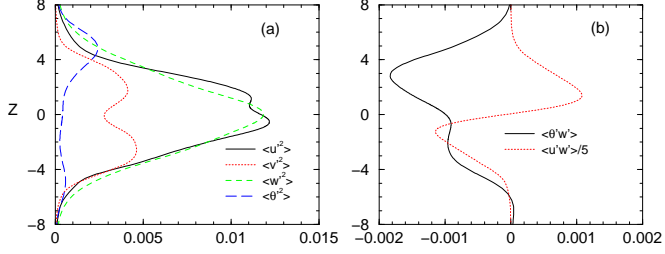
Figure 6: Profiles of variances and fluxes in the low Reynolds number DNS: (a) $\langle u'^2 \rangle$ (solid), $\langle v'^2 \rangle$ (dotted), $\langle w'^2 \rangle$ (dashed), $\langle \theta'^2 \rangle$ (long-dotted) (b) $\langle \theta' w' \rangle$ (solid), $\langle u' w' \rangle$ (dotted).

though the peaks of $\langle u'^2 \rangle$ in the low Reynolds number DNS does not agree with the closure model result, it is curious to note that the behavior of $\langle u'^2 \rangle$ in the closure model and that of the higher Reynolds number DNS results, reported in Fig. 3a, are compatible. From Fig. 9, we find that multiple branches in the scaling of Ri_f versus Ri_g is reproducible even in this simple second-order closure model.

The results for various budgets, from the closure model, are shown in Fig. 10. Although magnitudes of various terms do not exactly match DNS results, much of the vertical variability is captured reasonably. Further improvements in the modeling of transport terms appear to be the first priority. The DNS transport terms, split into viscous (diffusive) part, turbulent (triple-moment) part and pressure part, are shown in Fig. 11. Note that although the total transport term is a loss on either side of the jet and is transferred from these shear zones to the core and outer regions of the jet, a curious feature can be noticed from the profile of triple-moment transport term in the equation for the vertical velocity variance. It shows a loss in the innermost core of the jet and gains on either sides of the jet in the shear zones. This result implies a two-way exchange of kinetic energy (or variances) between the shear production zones and the innermost core of the jet. The DNS results shows that pressure transport terms, in the vertical velocity variance and heat flux budget equations, have an out-of-phase relation with the triple moment transport term. The former is expected to have a significant contribution from wave dynamics, which may need to be
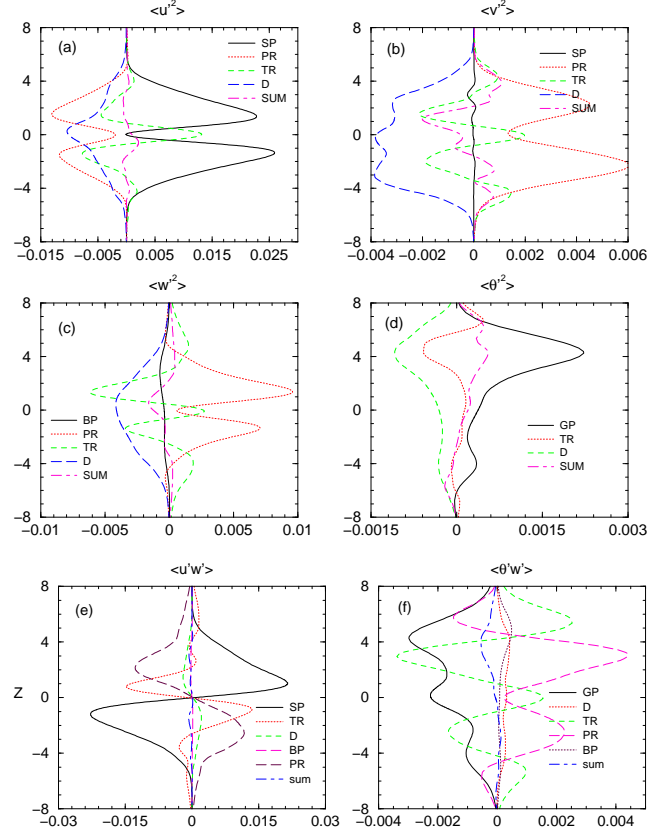

Figure 7: Budgets of variances and fluxes from the DNS: (a) $\langle u'^2 \rangle$ (b) $\langle v'^2 \rangle$ (c) $\langle w'^2 \rangle$ (d) $\langle \theta'^2 \rangle$ (e) $\langle u' w' \rangle$ (f) $\langle \theta' w' \rangle$. Notations used in legends: SP-shear production, PR-pressure-strain/scrambling, TR-transport (or diffusion), D-dissipation, BP-buoyancy production, GP-gradient production.
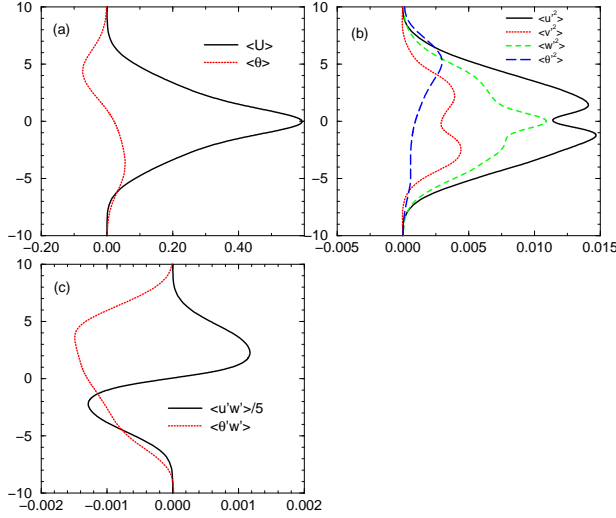
Figure 8: Profiles from the second-order closure model: (a) means $\langle U \rangle$ (solid), $\langle \theta \rangle$ (dotted) (b) variances $\langle u'^2 \rangle$ (solid), $\langle v'^2 \rangle$ (dotted), $\langle w'^2 \rangle$ (dashed), $\langle \theta'^2 \rangle$ (long-dotted) (c) $\langle \theta'w' \rangle$ (dotted), $\langle u'w' \rangle$ (solid).
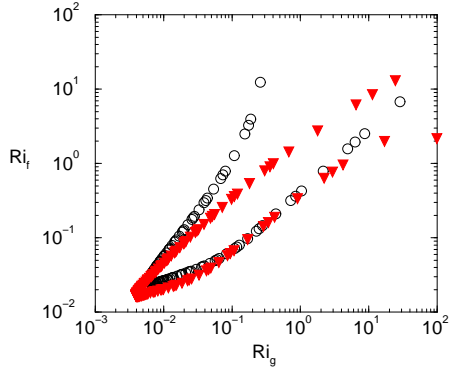

Figure 9: Scaling of flux Richardson number (Ri_f) with gradient Richardson number (Ri_g) in the closure model. Data points with $Z > 0$ are circles, and those with $Z < 0$ are triangles.

modeled independently. More sophisticated modeling of triple-moment transport, incorporating mean shear and buoyancy contributions, are also likely important for further improvement of the present closure model.

5. Conclusions

The formation of N^2-notch, found in our DNS, within the core of the turbulent jet is a physically interesting configuration favoring emission of gravity waves from shear-instabilities. We expect such waves to be more prominent in more realistic anelastic simulations with radiation boundary conditions at the top, and some form of horizontal inhomogeneities in the forcing. N^2-bulges found at edges of mixing layers may also be viewed as another plausible explanation of multiple tropopauses (viewed here as localized high gradients in potential temperature) in observations. In strongly turbulent jet, horizontal velocity variances tend to peak in shear zones on either sides of the jet, and the peak in vertical velocity variance is collocated with the jet maximum. Wave dynamics appears to be significant in regions where the temperature variance peaks, which are located on outer edges of the jet. While shear length scales show minima within turbulent jet shear zones, buoyancy related length scales peak there. The former increases with distance away from the jet, while latter decreases away from the jet. We also suggest that nonhomogeneous vertical stratification leads to multiple branches in the scaling of Ri_f with Ri_g, a result which can be utilized to improve turbulent mixing parameterization schemes near the tropopause.

We were able to obtain a DNS dataset with nearly balanced budgets for variances and fluxes, an ideal testbed to evaluate turbulence closure parameterizations. A closer look at individual terms in the transport (diffusion) terms in the budget equations of variances, revealed a two-way transport of TKE (variance) between shear production zones and innermost core of the jet. This fact will remain obscure if one merely considers a single budget equation for TKE. Preliminary evaluation of a simple second-order closure scheme suggested that better modeling of the out-of-phase relationship between pres-
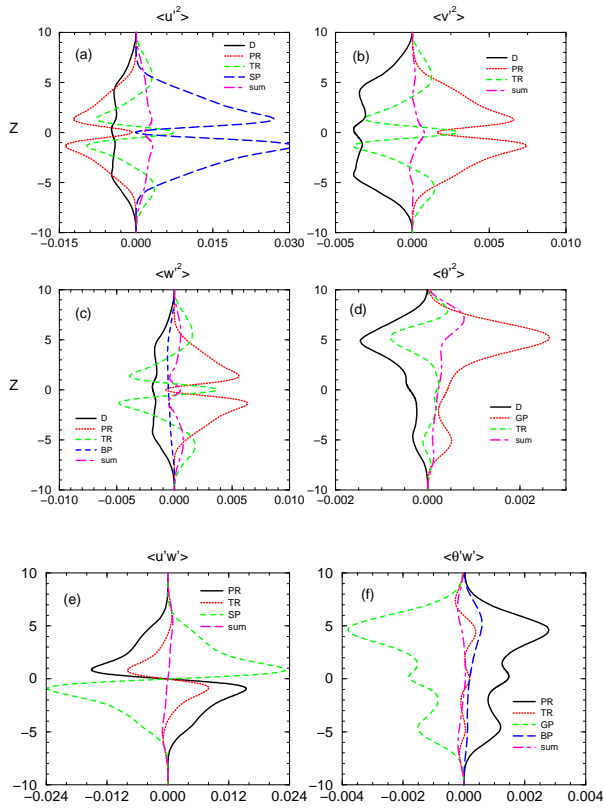
Figure 10: Budgets of variances and fluxes from the closure model: (a) $\langle u'^2 \rangle$ (b) $\langle v'^2 \rangle$ (c) $\langle w'^2 \rangle$ (d) $\langle \theta'^2 \rangle$ (e) $\langle u'w' \rangle$ (f) $\langle \theta'w' \rangle$. Notations are the same as in Fig. 7.
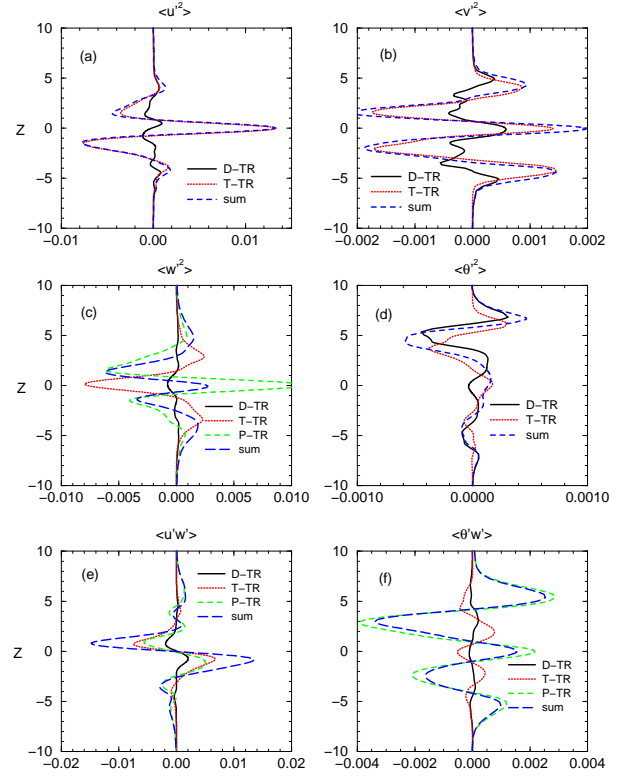
Figure 11: Splitting of transport term (TR) in the DNS budgets for: (a) $\langle u'^2 \rangle$ (b) $\langle v'^2 \rangle$ (c) $\langle w'^2 \rangle$ (d) $\langle \theta'^2 \rangle$ (e) $\langle u'w' \rangle$ (f) $\langle \theta'w' \rangle$. Notations used are D-TR for diffusive (viscous) transport, T-TR turbulent (triple-moment) term, and P-TR for pressure transport.

sure transport and triple moment terms in the budget equations for $\langle w'^2 \rangle$ and $\langle \theta' w' \rangle$ may be required for improved results.

References

Bedard, A.J. Jr., F. Canavero, and F. Einaudi: 1986, Atmospheric gravity waves and aircraft turbulence encounters. *J. Atmos. Sci.*, **43**, 2838–2844.

Chasnov, J. and K. L. Tse: 2001, Turbulent penetrative convection with an internal heat source. *Fluid Dyn. Res.*, **28**, 397–421.

Eaton, F. D. and G. D. Nastrom: 1998, Preliminary estimates of the vertical profiles of inner and outer scales from White Sands Missile Range, New Mexico, VHF radar observations. *Radio Sci.*, **33**, 895–903.

Lott, F., H. Kelder, and H. Teitelbaum: 1992, A transition from Kelvin-Helmholtz instabilities to propagating wave instabilities. *Phys. Fluids A*, **4**, 1990–1997.

Mellor, G.L. and T. Yamada: 1982, Development of a turbulence closure model for geophysical fluid problems. *Rev. Geophys. Space Phys.*, **20**, 851–875.

Muschinski, A.: 1997, Turbulence and gravity waves in the vicinity of a midtropospheric warm front: A case study using VHF echo-intensity measurements and radiosonde data. *Radio Sci.*, **32**, 1161–1178.

Phillips, O.M.: 1991, The Kolmogorov spectrum and its oceanic cousins: a review. *Proc. R. Soc. Lond. A*, **434**, 125–138.

Reed, R. J.: 1969, A study of the relation of clear air turbulence to the mesoscale structure of the jet stream region. *Clear Air Turbulence and its Detection*, Y-H. Pao and A. Goldberg, Eds., Plenum, New York, 287–307.

Sutherland, B. R., and W. R. Peltier: 1995, Internal gravity wave emission into the middle atmosphere from a model tropospheric jet. *J. Atmos. Sci.*, **52**, 3214–3235.

Tse, K. L., A. Mahalov, B. Nicolaenko, and H. J. S. Fernando: 2001, A spectral domain decomposition method and its application to simulations of shear-stratified turbulence. *Lecture Notes in Physics, 566*, J. L. Lumley Ed., Springer-Verlag, Berlin, 353-378.